The relationship between the fracture toughness and grain boundary characteristics in hot-dip galvanized zinc coatings

G Vincent, N Bonasso, J.S. Lecomte, B Colinet, B Gay, C Esling

The relationship between the fracture toughness and grain boundary characteristics in hot-dip galvanized zinc coatings

G. Vincent[1] N. Bonasso[1], J. S. Lecomte[1], B. Colinet[2], B. Gay[3], C. Esling[1,*]

[1] **Laboratoire d'Etude des Textures et Application aux Matériaux (LETAM),** CNRS UMR 7078, Université de Metz, F-57012 Metz Cedex 1, France

[2] **Recherche et Développement de Cockerill Sambre,** Groupe Arcelor, Campus Universitaire de Sart Tilman, B-4000 Liège, Belgique

[3]**Umicore Recherche,** Kasteelstraat 7, B-2250 Olen, Belgique

***Corresponding author.**

E-mail adresses : claude.esling@univ-lorraine.fr

Abstract

This publication presents an experimental study on the relation between the grain boundary (GB) characteristics and the intergranular cracking resistance in a hot dip zinc coating. The cracking was studied using in situ tensile tests in a scanning electron microscope on small tensile samples of a hot dip galvanized steel sheet. In situ testing offered a series of advantages like monitoring the kinematical evolution of cracking without unloading, or making micrographs and OIM imaging on the same area of the tensile sample. The grain boundaries were classified into random and special boundaries (respectively Low angle boundaries and Coincidence site lattice—CSL boundaries). These special boundaries which account for 3.5% of the whole boundaries clearly show better cracking resistance than the random boundaries. The only special boundaries which present cracking failure are in an orientation with their normal direction close to the tensile direction, i.e. submitted to a maximum effective stress. The grain boundaries characteristics are obtained from EBSD individual orientation measurements.

Introduction

Zinc coatings are anti-corrosion protective through cathodic protection. Hot dip galvanizing is the most current coating process [1]. Solidification cracks may appear in the zinc layer during its solidification on the steel substrate [2].
However the most significant cracking occurs at the later working of the material. According to whether the material is loaded in uniaxial tension—as in this study—or in biaxial expansion, the main cracking type is respectively intergranular or intragranular (cleavage) [3, 4]. It is well established that the grain boundary (GB) properties depend on the GB type, both in cubic [5, 6] and hexagonal materials [7]. The cracking resistance of special GBs has also been studied by percolation modeling [8]. The aim of the present work is to study the relation between intergranular cracking and the distribution of GB types in a polycrystalline zinc layer by in situ uniaxial tensile tests in the chamber of a scanning electron microscope.

Experimental procedure

Material used

The zinc coating studied has been prepared in a galvanizing simulator with a zinc bath containing 0.3% Al in weight. The industrial hot dip process is simulated in controlled atmosphere. Before entering the simulator, the steel substrate is cleaned. It is then quickly introduced in the simulator to avoid any pollution by atmospheric gases. Then it is fixed at the end of a sample rod where it is annealed for 45 s at 700 °C before being set at 465 °C, the inlet temperature of the zinc bath. The sample is dipped for 3 s in the zinc bath using the sample rod. It is dried in a nitrogen flow to control the final coating thickness and cooled down. The so obtained zinc coating (Fig. 1a) has a 10 µm thickness and a 60 µm average grain size (Fig. 1b). According to the specific grain size, we established the cartography of a (2.5 x 2) mm² area representative to the sample in the SEM. The orientation and misorientations statistics of the zinc grains were determined before deformation. The aim of these statistics is to establish the correlation between the cracks observed in the SEM and the misorientations across the grain boundaries or GB types obtained by EBSD.

In situ tensile tests

To study the deformation behavior of the coating, and more specifically intergranular cracking, we machined tensile specimens out of the sheet. These specimens—of small size (40 x 6 mm²)—were placed in the tensile testing machine MT100 of trade mark FONDIS which is used for the in situ mechanical testing in the SEM (LEICA 440). The tensile machine is used as sample holder, the tensile direction being parallel to the rolling direction. In addition it is equipped with a force meter and an incremental displacement transducer of the traverse glide, interfaced with a PC which records and plots the ‘‘Force–Displacement’’ curve. The cracks generated by the deformation were observed in the SEM.

Texture determination

The studied zinc coating, of hexagonal compact (hcp) structure, has a strong anisotropy. The distribution of grain misorientation is, to a large extent, a direct consequence of the distribution of grain orientations, i.e. of the crystallographic texture [9]. There is thus certainly a relation between texture and the cracking resistance of the galvanized coating [10]. To grasp this relation, we characterized the coating on various scales. A first approach consists in analyzing the global texture of the coating by polycrystalline X-ray diffraction. The pole figures (PFs) were measured with a X-ray diffractometer using the Co Kα line (λCo = 0.1789 nm) and an Fe filter from the incomplete (00.2), (10.0), (10.1) and (10.2) PFs measured up to a maximum 80tilt, the orientation density function ODF and the complete PFs figures were obtained by the harmonic method in Bunge’s formalism [11]. At the microscopic scale, in order to study the local orientations and misorientations across the grain boundaries of the zinc crystallites, we choose to analyze in the SEM the tensile-samples in the as-received state before deformation, then after successively 5 and 7% of tensile elongation. The EBSD orientation mappings were carried out on the same area—selected on the sample prior to deformation—which comprises a population of 1730 individual grains and 3721 grain boundaries.

Near coincident cells for hexagonal crystals

Grain boundaries are generally classified into random GBs and special GBs. This latter category comprises the low angle boundaries Σ1 and the coincidence site lattice Si CSL boundaries. Various studies showed that these CSL boundaries show improved properties to

an upper limit of the coincidence index set to i = 29 in the case of cubic crystal symmetry [12, 13]. In the present study for hcp crystal symmetry, this corresponds to an upper limit of 28, so that we restricted the statistical study to the Si CSL for i = 1–28. To visualize the geometry of the CSL lattice, one can think of two interpenetrating crystal lattices. These crystal lattices share a common node and are disorientated to each other by a rotation around an axis passing through this common node. When the two lattices share at least one additional node, they have in fact a common super-lattice of coincidence. The value of Σ is defined by the ratio of the volume of the superlattice cell to the initial lattice cell. In polycrystals, misorientations across the CSL GBs generally present a deviation compared to the exact value resulting from the lattice geometry. Indeed intergranular dislocations appear systematically to decrease energy due to that deviation. The commonly accepted deviation criterion is that of Brandon (Eq. 1) [14],

$$\upsilon_m = \frac{\upsilon_O}{\sqrt{\Sigma}} \qquad (1)$$

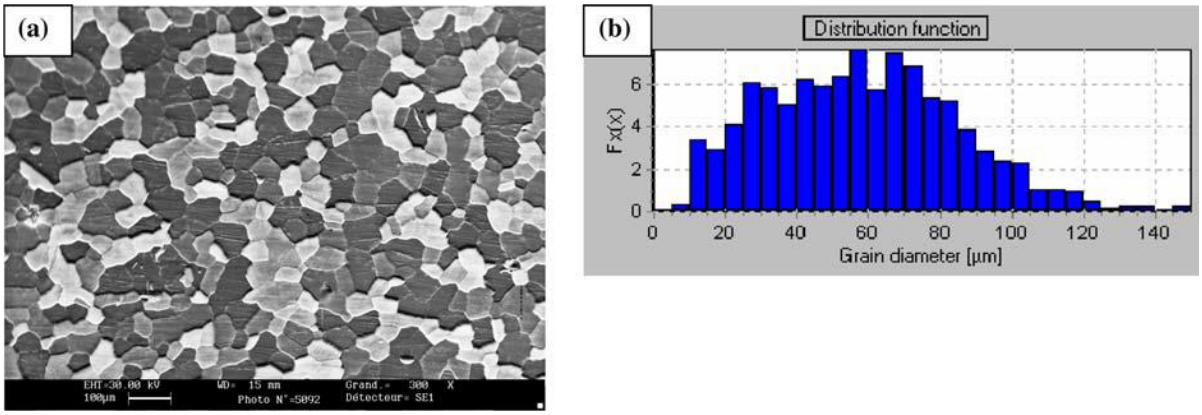

Fig. 1 *(a) SEM microstructure of the 10 µm-thick zinc coating observed after Finkeldey-solution etching (b) Grain size distribution (for a total of 1730 grains) in a (2.5 x 2) mm² area of the galvanized zinc coating. The mean grain size is 58 µm*

where υ_O is the angular limit to a subgrain boundary and υ_m the angular limit corresponding to a Σi of order i. The angular limit for low angle boundaries Σ = 1 (identity) corresponding to the maximum angular deviation υ_O was set to 15 for cubic crystal lattice. The angular deviation criterion for the CSL boundaries is not always applied in the original definition given by Brandon, but in alternatives, in particular for specific alloys [15]. We set the value m0 equal to 10° instead of the 15° generally adopted in the case of cubic symmetry [16]. In the hexagonal crystalline system of zinc, a 10 rotation around the highest order A6 axis accounts for 1/6 of the corresponding asymmetric unit, just as in the cubic system a 15 rotation around the highest order A4 axis accounts for 1/6 of the corresponding asymmetric unit. It appeared that this choice of 10° led to more coherent results on the improved properties of the CSL GBs. Watanabe suggested the subtle distinction between structure related and physical property related deviation criterions, and to insert the angular deviation from exact CSL misorientation of cracked CSL boundaries in a chart of Brandon type deviation curves for various m0 values (Fig. 2).

To draw up the list of the CSL GBs, we based on the table of quasi coincidence ‘‘near CSL’’ published by Bonnet et al. [17], selecting reasonable rational approximants $(n/m)^2$ (n and m integers) for the $(c/a)^2 \approx 3.445$ ratio of the zinc hcp lattice. Table 1 gives the rotation axis <uvw> and angle θ_D of the lattice misorientation of the through the CSL boundary as well as the angular tolerance mm calculated as indicated above, up to the coincidence order 25. We carried out independent calculations with an original algorithm that allowed to complete this

table by two additional CSL boundaries Σ27* and Σ28*. The fully completed table (Table 1) has been taken into account when analyzing the experimental results. Our program calculating the misorientations is based on previous work of Heinz and Neumann [18]. Starting from the EBSD orientation of two neighboring grains, it calculates their misorientation and to compares it with the characteristic CSL misorientations of zinc given in Table 1. Among the symmetry equivalent misorientations, we choose by convention the axis–angle couple corresponding to the minimum misorientation angle. The calculation program uses two reference frames: a macroscopic frame related to the sheet and a microscopic reference mark related to each individual grain. The rotation mapping the microscopic to the macroscopic reference frame can be parameterized, for example, by the Euler matrix M_{ij} and the Euler angles (ϕ_1, Φ, ϕ_2) (Eq. 2).

$$M_{ij} = \begin{pmatrix} a_{11} & a_{12} & a_{13} \\ a_{21} & a_{22} & a_{23} \\ a_{31} & a_{32} & a_{33} \end{pmatrix}$$

$$\begin{aligned} a_{11} &= \cos\phi_1 \cos\phi_2 - \sin\phi_1 \sin\phi_2 \cos\Phi \\ a_{12} &= \sin\phi_1 \cos\phi_2 + \cos\phi_1 \sin\phi_2 \cos\Phi \\ a_{13} &= sin\phi_2 \, sin\,\Phi \\ a_{21} &= -\cos\phi_1 \sin\phi_2 - \sin\phi_1 \cos\phi_2 \cos\Phi \\ a_{22} &= -\sin\phi_1 \sin\phi_2 + \cos\phi_1 \cos\phi_2 \cos\Phi \\ a_{23} &= cos\phi_2 \, sin\,\Phi \\ a_{31} &= \sin\phi_1 \sin\Phi \\ a_{32} &= -\cos\phi_1 \sin\Phi \\ a_{33} &= cos\,\Phi \end{aligned} \qquad (2)$$

The misorientation between two grains—or between the two reference frames linked to them—can be defined in the following way [18] (Eq. 3):

$$\Delta G_{ij} = g_j \cdot g_i^{-1} = g_j \cdot g_i^T \qquad (3)$$

where g_i and g_j represent the respective orientations of the two grains.
The matrix representation of the misorientation ΔG_{ij} is not unique because of the crystal symmetry. It is thus necessary to introduce two symmetry operators S^k and S^l [19] into the expression (Eq. 3) of misorientation ΔG_{ij} between the two crystals:

$$\Delta g_{ij} = S^k \Delta G_{ij} \, (S^l)^T \qquad (4)$$

The misorientation angle ω_G is deduced straight forwardly from the trace $tr(\Delta g_{ij})$ of this matrix by:

$$\cos\omega_{ij} = \frac{\left[tr(\Delta g_{ij}) - 1\right]}{2} \qquad (5)$$

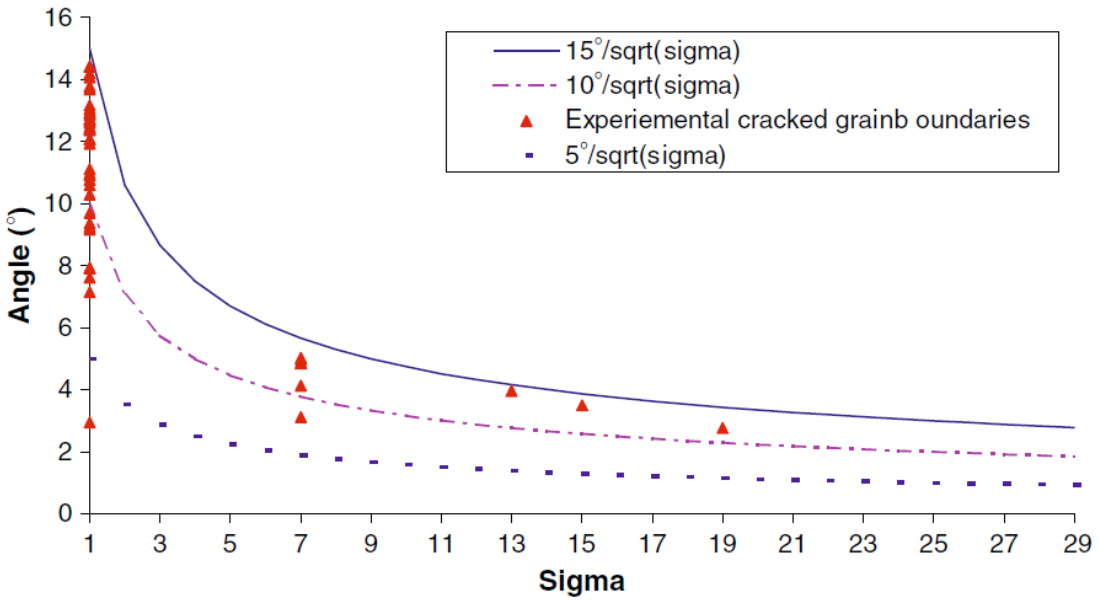

Fig. 2 *Angular deviation from exact CSL misorientation of cracked CSL boundaries inserted in a chart of Brandon type deviation curves for various υ_0 values*

Among the possible misorientations Δg_{ij} taking into account the multiplicity due to the crystal symmetries, the selection criterion will be the minimization of the misorientation angle $\omega_{\Delta G}$. This minimum angle will be compared with the theoretical misorientations angles provided by the CSL misorientation table.

The υ_m criterion (derived from the modified Brandon criterion) is introduced as tolerance on the misorientation angle, in particular to take into account uncertainties related to individual orientations measurements by EBSD. The deviation angle is calculated in the same way as before (Eqs. 6 and 7). The CSL misorientation matrix, M_{CSL}, is calculated starting from the theoretical misorientation angle θ_D and axis $<uvw>_{CSL}$ of the corresponding CSL in Table 1.

$$M_D = \Delta g_{ij} \cdot M_{CSL}^{-1} = \Delta g_{ij} \cdot M_{CSL}^{T} \tag{6}$$

$$\cos \gamma_D = \frac{[tr(M_D) - 1]}{2} \tag{7}$$

The condition for a GB being counted as a coincidence boundary is that the deviation angle γ_D be lower than the limit value υ_m set by the criterion:

$$\gamma_D \leq \upsilon_m \tag{8}$$

The program then makes it possible to draw a cartography of the GB misorientations by assigning a particular color to each CSL boundary type. In the following, we will regroup the grain boundaries with the same index *i* in CSL families denoted Σ i.

Table 1 Near coincident site lattice relations for Zn giving the misorientation axis *uvw* and angle θ_D of the lattices across the CSL Σ -boundary

$(n/m)^2$	Σ	*uvw*	θ_D	ν_m
Any	1	Any	0.00	10
Any	7	001	21.79	3.77
7/2	9	210	56.25	3.33
27/8	9	100	70.53	3.33
27/8	11	100	50.47	3.01
Any	13	001	27.80	2.77
7/2	13	100	85.59	2.77
24/7	15	100	86.18	2.58
21/8	15	100	29.93	2.58
7/2	15	210	29.93	2.58
7/2	15	210	86.18	2.58
27/8	15	210	78.46	2.58
7/2	17	100	49.68	2.42
27/8	17	100	86.62	2.42
Any	19	001	13.17	2.29
27/8	19	100	26.53	2.29
7/2	21	310	70.53	2.18
27/8	21	210	44.41	2.18
17/5	22	210	56.25	2.13
7/2	23	100	34.30	2.08
7/2	23	210	77.44	2.08
27/8	23	18 9 2	79.98	2.08
7/2	25	210	63.90	2.00
27/8	25	310	63.89	2.00
27/8	27*	100	38.94	1.92
69/20	28*	100	49.99	1.88

Results and discussion

Study of the orientations and misorientations of the grains

The global texture of the studied coating is a <*c*> axis fiber texture, the average orientation of the axes <*c*> being normal to sheet, with an angular spread of 15° to the normal direction DN (Fig. 3a–c).

The global texture does not give account for the local misorientation characteristics of misorientation between neighboring grains. Only determination of local texture gives access to the determination of the misorientation between grains.

Thus the orientation map (Fig. 4) represents the material at the microscopic scale of the grains. On this map (00.2) grains are mainly of dark colors, i.e. their <*c*> axes are perpendicular to the sheet plane, while the white zones of the map could not be indexed by EBSD. The grains boundaries pictured in white color are low angle boundaries of misorientation smaller than 10°. The various levels of gray confirm that the distribution of the orientations by rotation around the normal direction is homogeneous which confirms a complete fiber texture with < c> axis parallel to ND.

In view of these results, a significant number of special grain boundaries can be expected. Indeed it was confirmed, as seems reasonable, that a relatively marked fiber texture induces a significant number of misorientations whose axis is parallel to the fiber axis [20]. A fraction of these misorientations correspond to CSL boundaries with <*c*> as misorientation axis.

These latter CSL boundaries as well as those obtained by misorientation around other crystallographic axes are identified—within the limits of the angular tolerance υ_m—by comparison with the Σ boundaries listed in Table 1.
It is then easy to identify and to classify the grain boundaries into random and various CSL boundaries. Figure 5 presents part of the orientation micrograph on which the CSL boundaries have been identified and marked.
According to Table 2, 2.71% of the boundaries are low angle S1 boundaries, 1% are coincident CSL boundaries (Σ 7 to Σ 28) and 96.29% of random grain boundaries. Among the coincident boundaries, the Σ 7 and Σ 19 classes are in a majority. For this galvanized sheet the frequencies of the coincident boundaries in the zinc coating are definitely smaller than those determined by Kim and Al in a polycrystal of NiAl [21] (Σ 1 = 17%, Σ 3 = 1.1%, Σ 5 = 1.8%, Σ 7 = 0.4%). The variation observed can be explained by the lattice type (here hexagonal) and by the restriction of the angular tolerance which results from the restriction of Brandon's criterion.

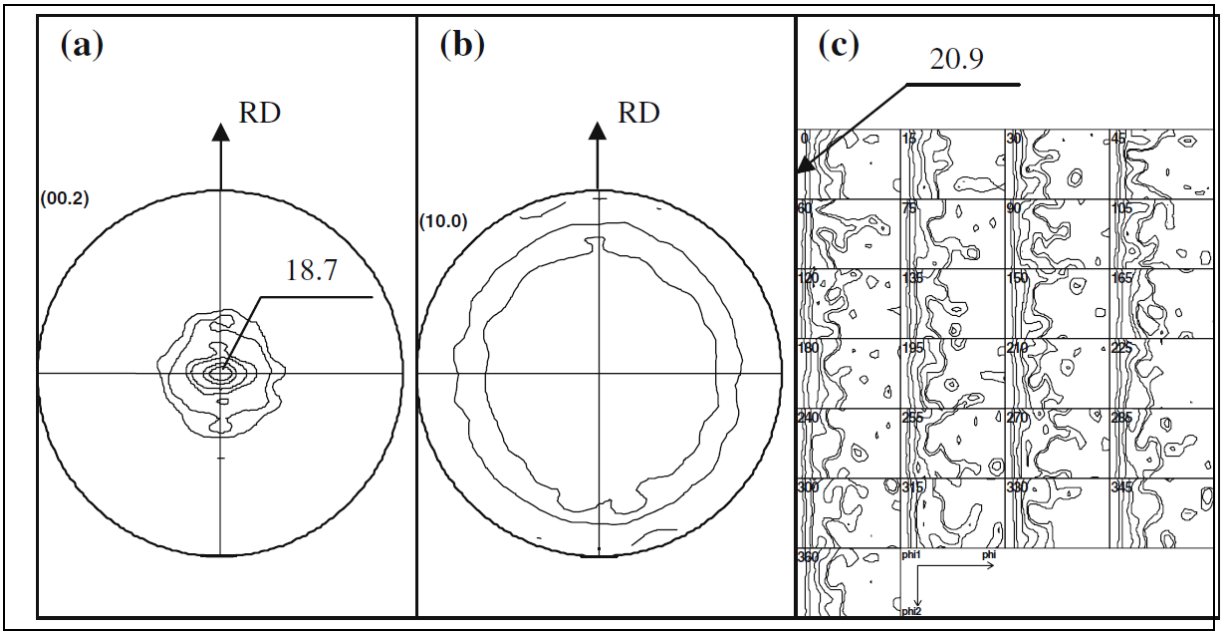

Fig. 3 *(a) Calculated (00.2), (b) (10.0) pole figures and (c) Orientation Density Function (ODF) of the hot-dip galvanized zinc coating*

It might be interesting to standardize the rates of special boundaries given in this textured sample by scaling them to the respective rates of special boundaries obtained for a random distribution of crystals of hexagonal symmetry.

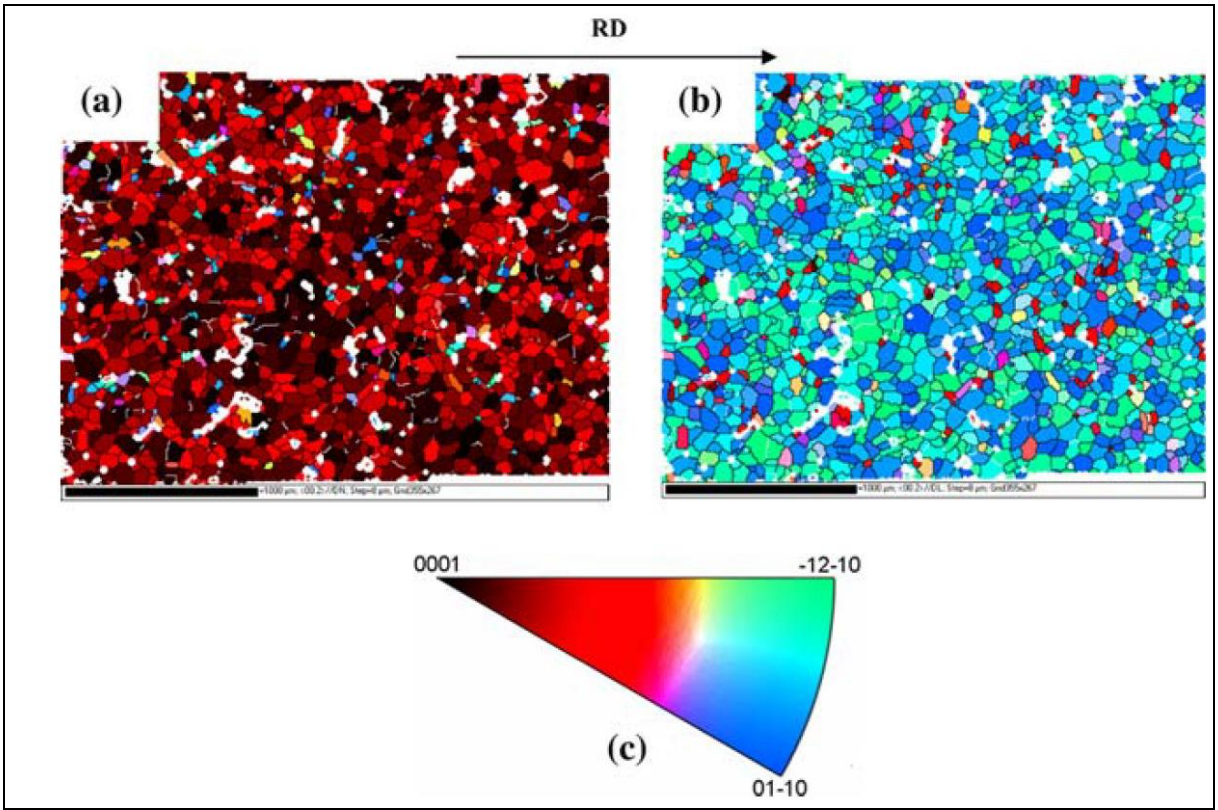

Fig. 4 *OIM map of the hot-dip galvanized zinc coating. The grains are colored according to (a) orientation of the ND direction in the standard triangle and (b) orientation of the RD direction in the standard triangle; (c) color code in standard triangle*

The distributions of misorientations for a random texture are generated according to the method suggested by Zuo and Esling [22] using two triplets of random numbers (r1 to r6) specifying sets of Euler angles for couples of grains A and B (Eq. 9):

$$\begin{aligned} \varphi_1^{\mathrm{A}} &= 2r_1\pi; \qquad \phi^{\mathrm{A}} = \cos^{-1}(1-2r_2); \qquad \phi_2^{\mathrm{A}} = 2\,r_3\pi; \\ \varphi_1^{\mathrm{B}} &= 2r_4\pi; \qquad \phi^{\mathrm{B}} = \cos^{-1}(1-2r_5); \qquad \phi_2^{\mathrm{B}} = 2r_6\pi; \end{aligned} \tag{9}$$

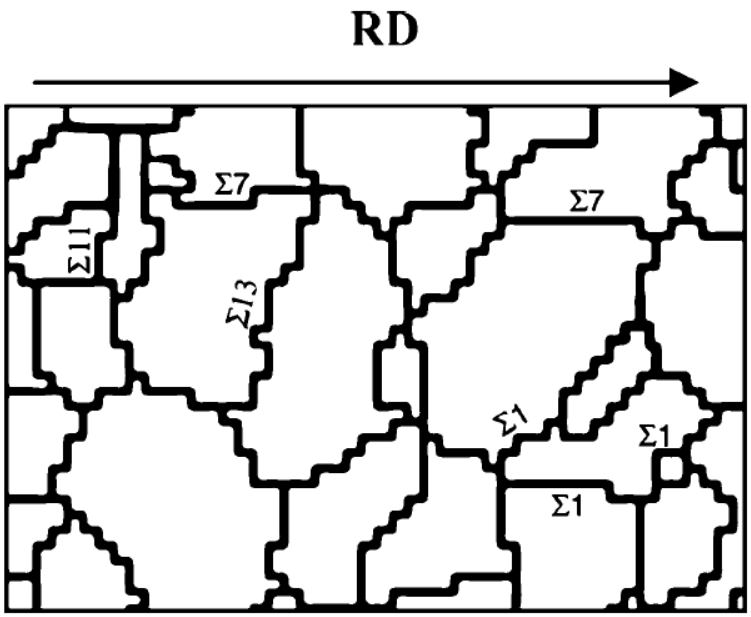

Fig. 5 *OIM micrograph of the hot-dip galvanized zinc coating. Coincident boundaries (S £ 28) are selected according to the Brandon-type criterion (Eq. 1) with m0 = 10°. Non-labeled boundaries are random grain boundaries*

Figure 6 confirms that the distribution of misorientations is strongly influenced by the texture type. We calculated the theoretical distribution of misorientations for a random polycrystal built with crystals of hexagonal symmetry, distribution which had been published in the case of crystals of cubic symmetry [23]. The difference between the two distributions for the random and textured sample is striking.

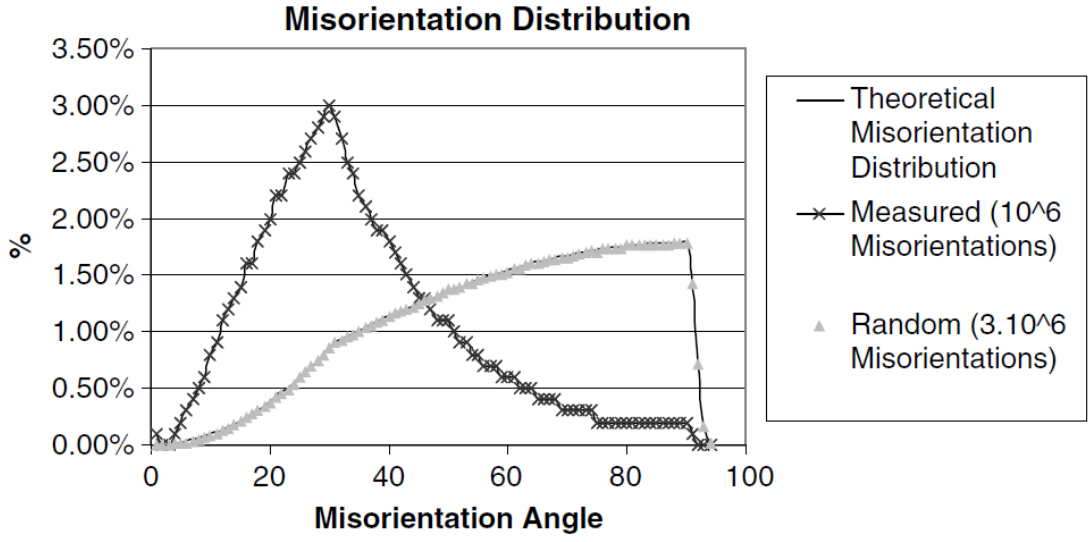

Fig. 6 *Distribution of misorientations for a random texture of hexagonal crystal symmetry generated from a statistical sample including 3 x 10^6 grain boundaries*

The experimental basal texture presents a sharp maximum localized at 30° whereas the theoretical distribution of misorientations is a monotonous increasing curve until its maximum obtained for a misorientation of 93.84°. This latter value is the maximum possible misorientation in the fundamental asymmetric unit for misorientations of crystals of hexagonal symmetry. The rates of special boundaries for a random distribution are given in Table 3. This table also reports the ratio $F_{rel.}$ of the actually measured frequencies of special boundaries to those calculated from the random distribution (Eq. 10):

$$F_{rel.} = \frac{F_{\Sigma_{exp}}}{F_{\Sigma_{isotrope}}} \quad (10)$$

Whereas the random boundaries and the coincident boundaries of Sigma 9, 15, 17, 21, 23 have a relative frequency close to the unit, the coincident boundaries of Sigma 1, 7, 11, 13, 19 have a raised relative frequency ranging from 2.96 (Sigma 11) to 10 (Sigma 7). The coincident boundaries of Sigma 22, 25, 27, 28 are not represented (relative frequency equal to 0). Besides they are almost non-existent in the random texture generated from 3 x 10^6 grain boundaries. The results are summarized in the Fig. 7.
It is well-known that the low angle boundaries Σ 1 and coincident CSL boundaries show a better cracking resistance than random boundaries for cubic materials [21]. We will check experimentally that this remains true in the case of hexagonal materials and in particular for a galvanized zinc layer.

Table 2 *Distribution of the grain boundaries in various types: low-angle and large angle boundaries, the latter being subdivided into random and CSL boundaries*

	Type of Σ boundary	GBs in the general population (in numbers)	GBs in the general population (in %)
Low-angle	Σ1	101	2.71
Large-angle	Σ7	14	0.38
	Σ9	3	0.08
	Σ11	3	0.08
	Σ13	3	0.08
	Σ15	3	0.08
	Σ17	1	0.03
	Σ19	8	0.21
	Σ21	1	0.03
	Σ22	0	0
	Σ23	1	0.03
	Σ25	0	0
	Σ27	0	0
	Σ28	0	0
	>Σ28	3583	96.29
Total		3721	100.00

Study of cracking behavior

We observed the sample before and after deformation by uniaxial tensile test carried out in situ in the SEM. On Fig. 8a–c, for an unpolished sample and before deformation, the grains have a dendritic structure. The grain boundaries are visible. After 5% of deformation they appear more marked since the grains underwent a slight rotation. Intergranular cracks appear, which is in conformity with former results of the literature [24] for an extensometric test. At 7% of deformation, the cracks, already present at 5% of deformation, continue to propagate towards other grain boundaries. In parallel to the propagation of already existing cracks, new cracks open. At high magnification (Fig. 8d), the first stages of grain decohesion can be observed.

It was already shown that certain types of grain boundaries show a better cracking resistance than others [21, 25]. In order to control the damage and thus the cracking of the coating, it is useful to identify the cracking resistant grain boundaries and to optimize the industrial process to promote their occurrence. To establish the relation between the GB characteristics and their cracking resistance, all the grain boundaries were first identified and numbered. These grain boundaries were then classified according to their GB character, their orientation with respect to the uniaxial stress and their cracking behavior. We calculated that the percentage of cracking boundaries is 11% for the random boundaries (395 cracked for a total of 3593 random boundaries) whereas it is only 7.2% for coincident CSL boundaries (10 cracked for a total of 138 CSL boundaries). Among the latter, 5.4% are CSL boundaries with Σ ranging between 7 and 28, and 7.9% low angle or Σ 1 boundaries. The cracking percentage for Σ 1 boundaries might seem relatively high at first sight, but it is necessary to take into account the large angular tolerance which is highest for Σ 1 boundaries with 10°, whereas it is only of 3.77° for Σ 7 boundaries (cf. Table 1). As a general rule, coincident CSL boundaries present an improved cracking resistance as compared to the random grain boundaries. The following paragraph will show that the orientation of the boundary compared to the direction of uniaxial traction i.e. the intensity of the effective normal stress component on the GB is very significant in the cracking behavior [8].

Table 3 *Frequency of CSL grain boundaries for a random texture of hexagonal crystalline symmetry and relative frequency (scaled to random) $F_{rel.}$ of CSL grain boundaries in the sample with basal texture*

Sigma	1	7	9	11	13	15	17	19
Isotrope Hex (%)	0.33	0.038	0.18	0.027	0.025	0.069	0.047	0.039
$F_{rel.}$	8.21	10	0.44	2.96	3.2	1.16	0.63	5.38
Sigma	21	22	23	25	27	28	>28	
Isotrope Hex (%)	0.085	0.04	0.089	0.068	0.014	0.014	98.8	
$F_{rel.}$	0.35	0	0.33	0	0	0	0.97	

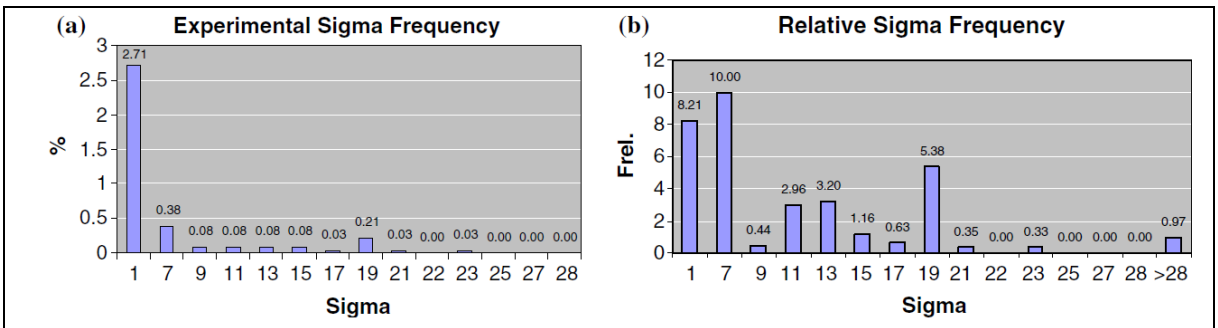

Fig. 7 (*a) Experimental Σ -Frequency and (b) Relative Σ -Frequency scaled to random texture*

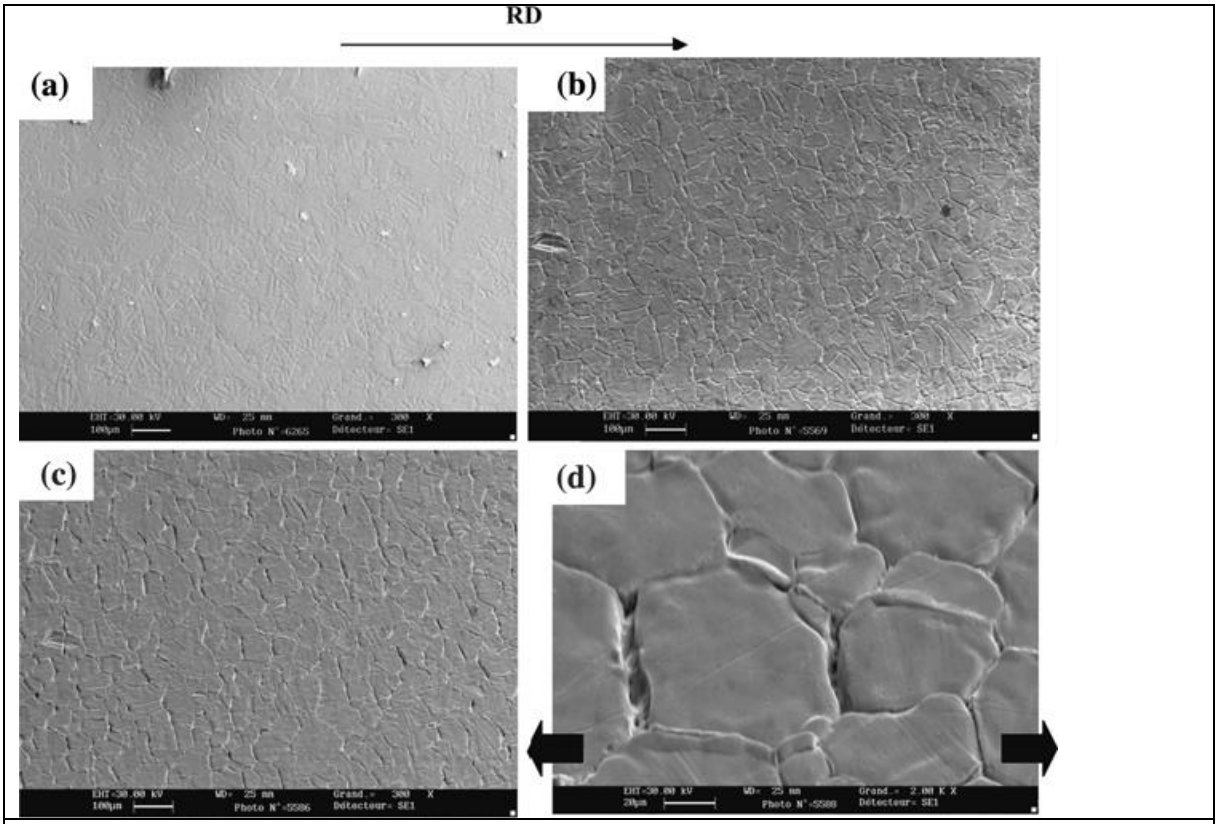

Fig. 8 *SEM micrographs of a tensile specimen of a zinc coated sheet (a) before traction, (b) after 5% of deformation, (c) after 7% of deformation and (d) zoom on the 7% deformed sample allowing to visualize intergranular cracking*

Correlation between the cracking behavior and the effective normal stress component

Each GB was classified with respect to the angle α between the normal <*n*> to the GB plane with the uniaxial tensile direction < TD> (Fig. 9). Nine angle classes a were defined by ranges of 10° width, from 0° to 10°, from 10° to 20° etc. For simple symmetry considerations, the asymmetric unit of variation of this angle ranges in the interval from 0° to 90°.
Figure 10 gives the distribution of the grain boundaries according to the angle α. There are two maximums in the ranges 0–10° and 80–90°, which corresponds respectively to grain boundaries perpendicular and parallel to the tensile direction, i.e. to the rolling direction of the steel substrate. This can be explained by the orthorhombic symmetry (or rectangular in plane symmetry) of the rolled sheet steel, as well as by effects of the sheet edges on the cooling conditions of the zinc layer. Between these two maximums, the orientations of the grain boundaries normals are distributed according to a Gaussian centered on 45°. That also shows that, as could be expect [26], that the working process (rolling) of the substrate influences the crystallization of the coating during cooling by inducing a characteristic distribution of the orientations of the grain boundaries planes. Distributions of the random grain boundaries (Fig. 11b) and of coincident CSL boundaries (Fig. 11a) according to the angle α present the same symmetry characteristics that have just been described for the whole set of all the grain boundaries. It appears that the percentage of cracked boundaries by orientation class is a monotonously decreasing function of the angle a for the random boundaries. Oppositely, in the case of CSL boundaries the decrease with the angle a is dramatic until the class 20–30°. Beyond this orientation class no CSL GB cracks because their resistance is high enough for the effective normal critical crack stress never be reached. These experimental results confirm

the interest of the theoretical and numerical model of intergranular crack propagation proposed by Wang et al. [8].

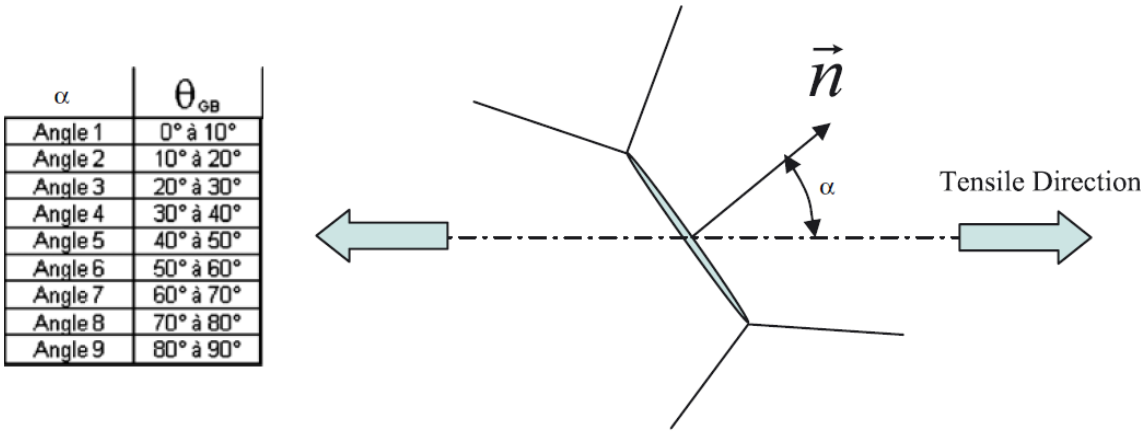

Fig. 9 *Orientation of the grain boundary plane with respect to the uniaxial tensile direction Nine angle classes α were defined from 10° to 10° in the angular range from 0° to 90°*

The analysis of cracking shows that the orientation class 0°–10° (Angle 1 on Fig. 11a, b) remains extremely unfavorable whatever the GB type. We observed the cracking at deformation rates amounting respectively to 5 and 7%. At this stage of extension, the critical cracking stress for the first grain boundaries to be cracked had then undoubtedly been exceeded. These first cracks were then propagate towards other grain boundaries (including S boundaries) stressed by local fields raised because of the stress redistribution within material as a consequence of the first cracks [8]. Oppositely when we consider all the other orientation classes from 10° to 90°, it appears that our results clearly confirm work performed on cubic crystals: CSL type boundaries prove an improved cracking resistance as compared to random boundaries. Even though this result was established for cubic crystals, there did not exist, to our knowledge, a similar work on hexagonal crystals. This result will also complement a study of the grain boundaries of a polycrystal of zinc deformed at high temperature [27].

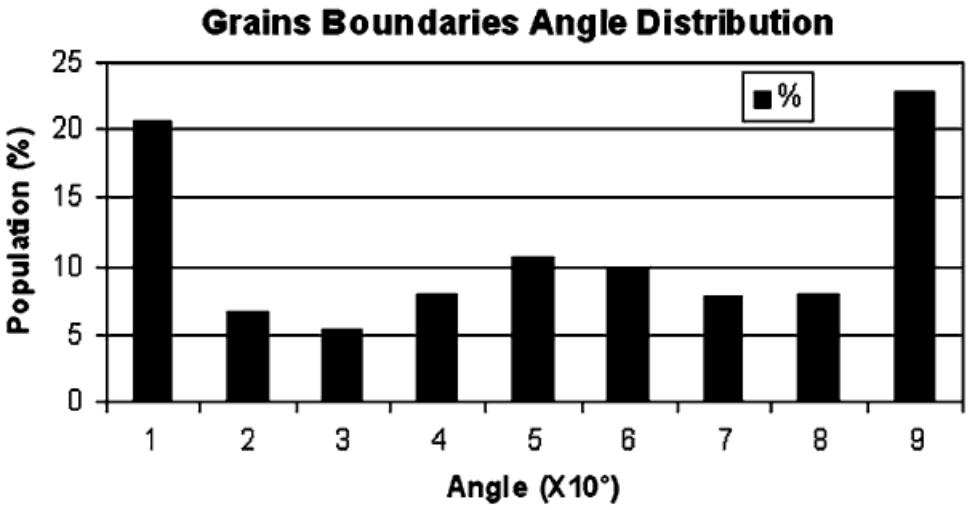

Fig. 10 *Distribution of the grain boundary orientations according to the angle α defined by the normal to the grain boundary plane and the direction of uniaxial tension*

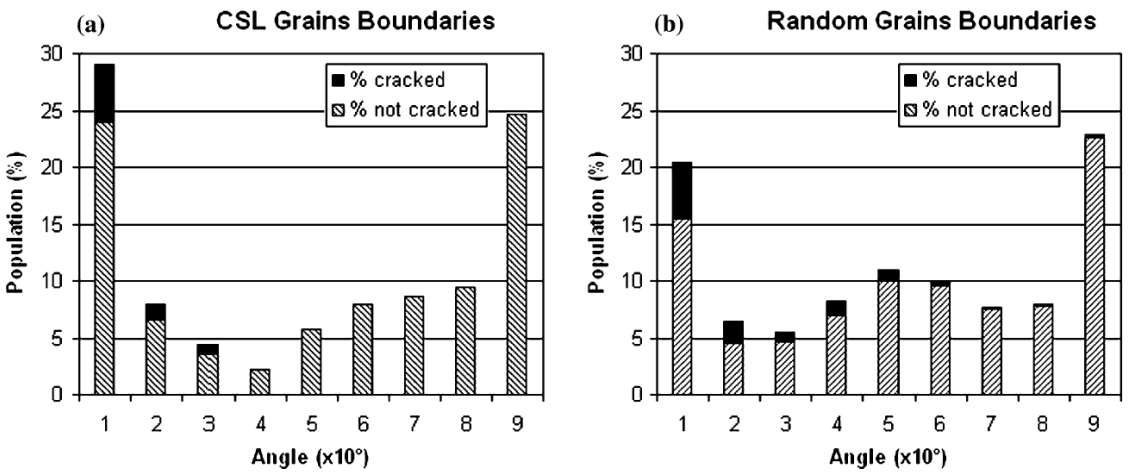

Fig. 11 *Distribution of the orientations of (a) CSL type grain boundaries (b) random grain boundaries. The orientations are defined by the angle a between the direction normal to the boundary plane and the direction of uniaxial traction. We also specified the percentage of cracked grain boundaries for each orientation class*

Conclusion

We studied the cracking resistance of the various types of grain boundaries in a galvanized zinc coating. For that we performed uniaxial tensile tests in situ in a SEM to establish a correlation between intergranular cracking and GB characteristics. We showed that CSL coincident boundaries are more resistant to cracking than random boundaries. The modification of Brandon's criterion (restriction of the deviation angle from 15° for cubic crystals to 10° for hexagonal crystals) seems to be a judicious and coherent choice which makes it possible to restrict the tolerance on the selection criterion for the CSL boundaries. The few CSL cracking boundaries correspond exclusively to the orientation class a. For the latter grain boundaries the angle of the GB normal to the tensile direction ranges between 0 and 30°, i.e. is directed almost perpendicular to the tensile direction. At this stage, it would seem that the critical cracking stress has been locally exceeded, in particular because of a possible redistribution of the local stresses following the cracking of most brittle grain boundaries. This is why to minimize the damage, it would be useful to increase the frequency of CSL coincident boundaries obtained right at the galvanizing process. It was shown in the literature that a heat treatment carried out on cubic materials increased considerably the fraction of the coincidence boundaries [19]. It should be thus possible on our alloy to increase the frequency of CSL coincident boundaries by an optimized heat treatment, taking into account the relatively low melting point of zinc (420°C) and avoiding increase in the grain size that would have a prejudicial effect.

References

1. Dunham KJ (2002) Metal Finish 100:20
2. Tzimas E, Papadimitriou G (2001) Technology 145:176
3. Lazik S, Esling C, Philippe MJ, Wegria J, Dubois M (1996) TMS 28:35
4. Parisot R, Forest S, Gourgues AF, Pineau A, Mareuse D (2000) Comp Mater Sci 19:189
5. Lim LC, Watanabe T (1990) Acta Metall Mater 38:2507
6. Watanabe T, Tsurekawa S (1999) Acta Metall Mater 47:4171
7. Watanabe T, Yamada M, Shima S, Karashima S (1979) Phil Mag A 40(5): 667

8. Wang G, Zuo L, Esling C (2002) Phil Mag A 12:2499
9. Beaujean I (1993) Ph.D. Thesis, University of Metz, Metz
10. Gaignard S, Lazik S, Lietzau J, Wegria J, Dubois M, Philippe MJ, Esling C (1999) TMS 34:147
11. Bunge HJ (1993) Texture analysis in material science, Cuvillier Verlag, Göttingen
12. Palumbo G, Aust KT, Lehockey EM, Erb U, Lin P (1998) Scripta Mat 38(11):1685
13. Gertsman VY, Zhilyaev AP, Szpunar JA (1997) Model Simul Mater Sci Eng 5:35
14. Brandon DG (1966) Acta Metall 14:1479
15. Pan Y, Adams BL, Olson T, Panayotou N (1996) Acta Metall 44:4685
16. Read WT, Shockley W (1950) Phys Rev 78:275
17. Bonnet R, Cousineau E, Warrington DH (1981) Acta Cryst A37:184
18. Heinz A, Neumann P (1991) Acta Cryst. A47:780
19. Humbert M, Wagner F, Moustafid H, Esling C (1995) J Appl Cryst 28:571
20. Zuo L, Watanabe T, Esling C (1994) Z Metallkde 85:554
21. Kim T, Hong KT, Lee KS (2003) Intermetallics 11:33
22. Zuo L, Esling C (1995) Scripta Metall Mater 32(6):937
23. Mackenzie JK, Thomson MJ (1957) Biometrika 44:205
24. Jaffrey D, Browne JD, Howard TJ (1980) Metall Trans B 11:631
25. Known JQ, Demura M, Hirano T (2003) Acta Materialia 51:2505
26. Lee DS, Ryoo HS, Hwang SK (2003) Mater Sci Eng A354:106
27. Watanabe T, Kimura SI, Karashima S (1984) Phil Mag A 49(6):845